residue of *Escherichia coli* outer-membrane phospholipase A is important for activity. *Eur. J. Biochem.* **234,** 934–938 (1995).
14. Brok, R. G. P. M., Ubarretxena-Belandia, I., Dekker, N., Tommassen, J. & Verheij, H. M. *Escherichia coli* outer membrane phospholipase A: Role of two serines in enzymatic activity. *Biochemistry* **35,** 7787–7793 (1996).
15. Dodson, G. & Wlodawer, A. Catalytic triads and their relatives. *Trends Biochem. Sci.* **23,** 347–352 (1998).
16. Ubarretxena-Belandia, I., Boots, J. W. P., Verheij, H. M. & Dekker, N. Role of the cofactor calcium in the activation of outer membrane phosphilipase A. *Biochemistry* **37,** 16011–16018 (1998).
17. Horrevoets, A. J. G., Hackeng, T. M., Verheij, H. M., Dijkman, R. & De Haas, G. H. Kinetic characterization of *Escherichia coli* outer membrane phospholipase A using mixed detergent-lipid micelles. *Biochemistry* **28,** 1139–1147 (1989).
18. Wei, Y. *et al.* A novel variant of the catalytic triad in the *Streptomyces scabies* esterase. *Nature Struct. Biol.* **2,** 218–223 (1995).
19. Ubarretxena-Belandia, I. *et al.* Outer membrane phospholipase A is dimeric in phospholipid bilayers: A cross-linking and fluorescence resonance energy transfer study. *Biochemistry* **38,** 7398–7405 (1999).
20. Blaauw, M., Dekker, N., Verheij, H. M., Kalk, K. H. & Dijkstra, B. W. Crystallization and preliminary X-ray analysis of outer membrane phospholipase A from *Escherichia coli*. *FEBS Lett.* **373,** 10–12 (1995).
21. Otwinowski, Z. & Minor, W. Processing of X-ray diffraction data collected in oscillation mode. *Methods Enzymol.* **276,** 307–326 (1997).
22. Kabsch, W. Automatic processing of rotation diffraction data from crystals of initially unknown symmetry and cell constants. *J. Appl. Crystallogr.* **26,** 795–800 (1993).
23. Collaborative Computational Project Number 4. The CCP4 suite: programs for protein crystallography. *Acta Crystallogr. D* **50,** 760–763 (1994).
24. Brünger, A. T. Free *R* value: a novel statistical quantity for assessing the accuracy of structures. *Nature* **355,** 472–475 (1992).
25. Jones, T. A., Zou, J.-Y., Cowan, S. W. & Kjeldgaard, M. Improved methods for building protein models in electron density maps and the location of errors in these models. *Acta Crystallogr. A* **47,** 110–119 (1991).
26. Kraulis, P. J. MOLSCRIPT: a program to produce both detailed and schematic plots of protein structures. *J. Appl. Crystallogr.* **24,** 946–950 (1991).
27. Merritt, E. A. & Bacon, J. A. Raster3D: photorealistic molecular graphics. *Methods Enzymol.* **277,** 505–524 (1997).
28. Nicholls, A., Sharp, K. A. & Honig, B. Protein folding and association: insights from the interfacial and thermodynamic properties of hydrocarbons. *Proteins Struct. Funct. Genet.* **11,** 281–296 (1991).
29. Esnouf, R. M. An extensively modified version of Molscript that includes greatly enhanced coloring capabilities. *J. Mol. Graphics* **15,** 132–134 (1997).

**Acknowledgements**

We thank the staff at the EMBL-outstation at DESY in Hamburg, and at the D2AM and the ID2B beam lines at ESRF Grenoble, for assistance with data collection. We thank R. L. Kingma for her enthusiastic collaboration and discussions. We thank the ESRF for supporting the work at the ESRF. These investigations were supported by the Netherlands Foundation for Chemical Research (CW) with financial aid from the Netherlands Organization for Scientific Research (NWO). We thank the EU for supporting the work at EMBL Hamburg through the HCMP Access to Large Installations Project.

Correspondence and requests for materials should be addressed to B.W.D. Coordinates have been deposited in the Protein Data Bank under accession numbers 1QD5 and 1QD6.

# The reaction cycle of isopenicillin *N* synthase observed by X-ray diffraction

**Nicolai I. Burzlaff*†, Peter J. Rutledge*†, Ian J. Clifton*, Charles M. H. Hensgens*, Michael Pickford‡, Robert M. Adlington*, Peter L. Roach* & Jack E. Baldwin***

* *The Dyson Perrins Laboratory and the Oxford Centre for Molecular Sciences, University of Oxford, South Parks Road, Oxford, OX1 3QY, UK*
‡ *The Laboratory of Molecular Biophysics, University of Oxford, South Parks Road, Oxford, OX1 3QY, UK*
† *These authors contributed equally to this work*

**Isopenicillin *N* synthase (IPNS), a non-haem iron-dependent oxidase, catalyses the biosynthesis of isopenicillin *N* (IPN), the precursor of all penicillins and cephalosporins[1]. The key steps in this reaction are the two iron-dioxygen-mediated ring closures of the tripeptide δ-(L-α-aminoadipoyl)-L-cysteinyl-D-valine (ACV). It has been proposed that the four-membered β-lactam ring forms initially, associated with a highly oxidized iron(IV)-oxo (ferryl) moiety, which subsequently mediates closure of the five-membered thiazolidine ring[2]. Here we describe observation of the IPNS reaction in crystals by X-ray crystallography. IPNS·$Fe^{2+}$·substrate crystals were grown anaerobically[3,4], exposed to high pressures of oxygen to promote reaction and frozen, and their structures were elucidated by X-ray diffraction. Using the natural substrate ACV, this resulted in the IPNS·$Fe^{2+}$·IPN product complex. With the substrate analogue, δ-(L-α-aminoadipoyl)-L-cysteinyl-L-*S*-methyl-cysteine (ACmC) in the crystal, the reaction cycle was interrupted at the monocyclic stage. These mono- and bicyclic structures support our hypothesis of a two-stage reaction sequence leading to penicillin. Furthermore, the formation of a monocyclic sulphoxide product from ACmC is most simply explained by the interception of a high-valency iron-oxo species.**

A challenge in protein crystallography is the possibility of directly observing the structural changes occurring in enzymes during the catalytic cycle. One approach has been the use of Laue crystallography, which has permitted the observation of relatively small changes in structure, such as the photodissociation of a small ligand[5]. The IPNS-catalysed oxidative synthesis of IPN involves significant movements of atoms, through the formation of the two fused heterocyclic rings of penicillin from the linear precursor ACV. Our approach involved the direct oxygenation of anaerobically grown crystals of IPNS complexed with $Fe^{2+}$ and substrates, then structural investigation by X-ray crystallography.

In solution, IPNS shows relatively slow kinetic parameters ($k_{cat} = 4.6\ s^{-1}$, $K_m = 0.56$ mM for ACV, where $k_{cat}$ is the maximum catalytic rate when substrate is saturating, and $K_m$ is the concentration of substrate at which the reaction rate is half its maximum value[6], and initial experiments with crystals exposed to atmospheric pressures of oxygen (air) proved unsuccessful. Therefore, a 'bomb' suitable for exposing crystals to oxygen at pressures up to 60 bar was built[7,8], and used to expose crystals of IPNS·$Fe^{2+}$·ACV to 40-bar oxygen for different time periods. After an exposure time of 20 min, a transient pale yellow colour ($\lambda_{max}$ 410 nm) was observed uniformly across the crystals; the colour faded with prolonged exposure and was no longer discernible after 320 min. The origin of this chromophore is at present uncertain, but a similar absorption ($\lambda_{max}$ 430 nm) has been attributed to a ferryl species in methane monooxygenase[9], although that enzyme has a di-iron centre.

A single crystal of IPNS·$Fe^{2+}$·ACV exposed to the same oxygen pressure for 320 min allowed determination of the structure of IPNS·$Fe^{2+}$·IPN to 1.35 Å resolution (Fig. 1a, b). The structure is primarily that of an IPNS·$Fe^{2+}$·IPN product complex, but residual electron density at the carbonyl and sulphide regions of the ACV cysteine unit make it apparent that the crystal still contains 30% of unreacted IPNS·$Fe^{2+}$·ACV (Fig. 1b). Attempts to obtain complete turnover by extended pressurization under oxygen (for up to 640 min) were unsuccessful. Crystals exposed for these longer times showed low occupancy in the substrate binding region, consistent with slow release of the product from the active site into the surrounding solvent.

The most significant differences between the IPNS·$Fe^{2+}$·IPN structure and the IPNS·$Fe^{2+}$·ACV complex are in the positions of the β-lactam carbonyl group and the cysteinyl sulphur atom. The carbonyl group has moved 60° around the axis of the cysteinyl $C_1$–$C_2$ bond, towards Phe 211. The absence of well-ordered hydrogen bonds to this carbonyl group in the substrate complex appears necessary to facilitate this movement. During the reaction, the sulphur migrates around the iron towards the valine β-carbon and out of the site *trans* to His 270, forming the pentacoordinate product complex. A cavity apparent in the IPNS·$Fe^{2+}$·ACV complex accommodates the sulphur in the product structure. The valine isopropyl group has rotated about the $C_\alpha$–$C_\beta$ bond to facilitate formation of the carbon–sulphur bond, and this rotation reverses

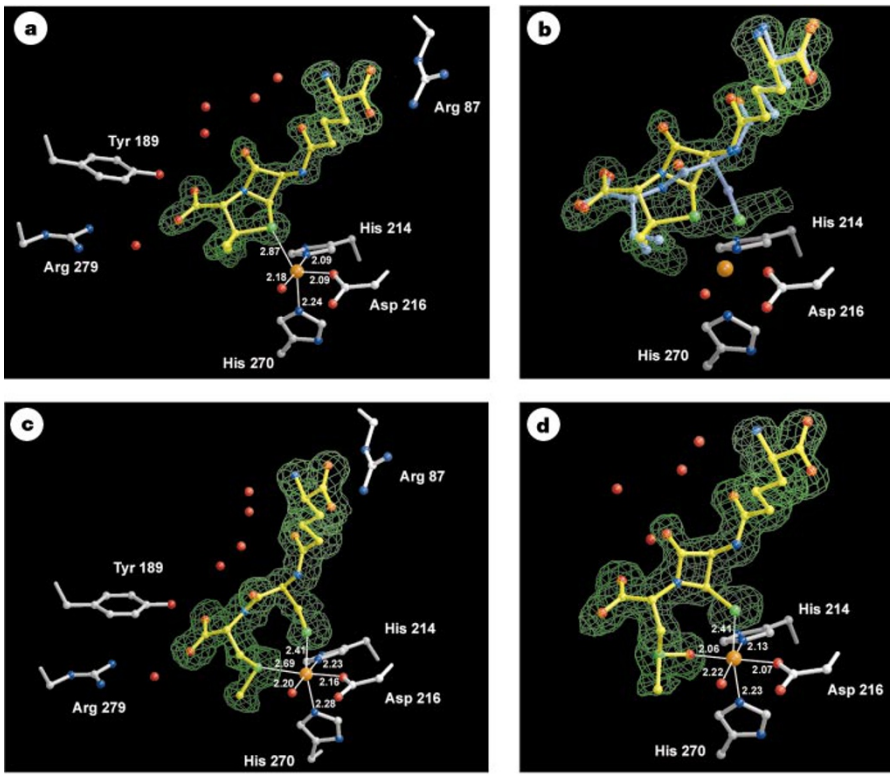


**Figure 1** Structures showing changes in the active-site region. All electron-density maps are contoured at 1σ; distances are shown in Å. **a**, The IPN model with an electron-density map ($2m(10/7(F_o - 0.3F_{cACV})) - DF_c$) of the IPN portion (70%). **b**, The mixed IPN and ACV model with a ($2mF_o - DF_c$) electron-density map. **c**, The IPNS·$Fe^{2+}$·ACmC structure before exposure to high-pressure oxygen, with a ($2mF_o - DF_c$) electron-density map. **d**, The IPNS·$Fe^{2+}$·ACmC structure after 10-min exposure to oxygen, showing the monocyclic sulphoxide product and a ($2mF_o - DF_c$) electron-density map. *m*, figure of merit; *D* approximates to the fraction of the calculated structure factor that is correct.

the position of the methyl groups bound to it, as thiazolidine formation is known to proceed with retention[10] (Fig. 1a, b).

The IPNS·$Fe^{2+}$·IPN structure also provides some evidence concerning product release from the active site. The IPN carboxylate groups derived from the aminoadipoyl side chain and valine remain tethered to the protein. Thus the penicillin, shortened relative to ACV, accommodates less well the three-point attachment to Arg 87, Tyr 189 and iron, and is presumably therefore 'activated' towards dissociation from the active site.

In parallel with our attempts to generate and characterize the bicyclic product in the active site of IPNS crystals, we designed a modified substrate that could, in principle, interrupt the reaction cycle at the monocyclic stage. There is much indirect evidence to support a mechanism involving a monocyclic β-lactam intermediate[2,11], possibly coupled to an iron(IV)-oxo species (Fig. 2, **2**) en route to the enzyme-product complex (Fig. 2, **3**). Given this, and the ease with which IPNS accommodates changes in the valine moiety of ACV[11], we selected the modified peptide ACmC as a substrate analogue potentially able to interrupt the reaction cycle as required. The only structural change from ACV is replacement of D-valine (Fig. 2, **1**) by D-*S*-methyl-cysteine (Fig. 2, **4**), and our plan was to intercept the proposed iron(IV)-oxo species (Fig. 2, **5**) by oxygen transfer to the methyl sulphide group, generating a sulphoxide product (Fig. 2, **6**). This is a known reaction of sulphides with metal-oxo species[12].

The modified peptide ACmC was crystallized anaerobically with IPNS and $Fe^{2+}$, and the structure of IPNS·$Fe^{2+}$·ACmC was determined to a resolution of 1.50 Å. The substrate analogue binds in a similar manner to ACV (Figs 1c and 3), being tethered by a salt bridge to Arg 87, by hydrogen bonding to Tyr 189, Arg 279 and Ser 281, and to the iron atom through its cysteinyl sulphur. However, whereas the iron is pentacoordinate in the IPNS·$Fe^{2+}$·ACV complex, in this structure the metal is hexacoordinate: the sulphur of the *S*-methyl moiety is bound in the proposed oxygen binding site, *trans* to Asp 216 (ref. 4). The iron–sulphur bond length is 2.69 Å for the sulphide, compared to the 2.41 Å observed for the cysteinyl sulphur–iron distance.

Despite this ligation of the sulphide in the putative oxygen binding site, the application of high-pressure oxygen brought about turnover in the active site of the IPNS·$Fe^{2+}$·ACmC crystals. The crystals were exposed to 20-bar oxygen for a wide range of time periods, and ten minutes proved optimal. The resulting X-ray structure, processed to a resolution of 1.45 Å, clearly shows essentially complete conversion to a monocyclic β-lactam species in the active site of IPNS (Fig. 1d).

We note that the carbonyl oxygen of the β-lactam has moved to a position similar to that seen in the IPNS·$Fe^{2+}$·IPN structure, whereas the cysteinyl sulphur atom occupies an almost identical position to that seen in the starting material. Changes in the region of the *S*-methylcysteinyl side chain are consistent with the formation of a metal-bound sulphoxide product. When the monocyclic β-lactam sulphonide (Fig. 2, **6**) was fitted to this density, the result was a structure with an oxygen–sulphur distance of 1.47 Å and an iron–oxygen distance of 2.06 Å (Fig. 1d). This structure of exposed IPNS·$Fe^{2+}$·ACmC provides direct evidence for the initial formation of a monocyclic β-lactam species in the reaction cycle of IPNS. Additionally, although we have not directly observed the iron(IV)-oxo species, observation of the sulphoxide directly bound to iron in the site *trans* to Asp 216, the postulated oxygen binding site[4], is in accord with the intermediacy of a ferryl oxygen species.

It is significant that in both the bicyclic and monocyclic structures the carbonyl oxygen atom of the β-lactam ring is hydrogen-bonded to two well ordered water molecules. In contrast, the corresponding carbonyl oxygen atom in the substrate structures has no hydrogen-bonding interactions with the enzyme or with well ordered water molecules. Such hydrogen bonds to the cyclized structures would

**Table 1 Data collection and statistics**

| | IPNS.$Fe^{2+}$.IPN | | IPNS.$Fe^{2+}$.ACmC | | IPNS.$Fe^{2+}$.ACmC | |
|---|---|---|---|---|---|---|
| Exposure to oxygen | 320 min, 40 bar | | Unexposed | | 10 min, 20 bar | |
| X-ray source | BW7B, EMBL, Hamburg | | 9.6, SRS, Daresbury | | BW7B, EMBL, Hamburg | |
| Wavelength λ (Å) | 0.8345 | | 0.8700 | | 0.8382 | |
| $R_{cryst}$ (%)* | 13.1 (8–1.35 Å) | | 17.3 (25–1.50 Å) | | 13.3 (8–1.40 Å) | |
| $R_{cryst}$ (%)* ($I/\sigma I > 2$) | 10.5 | | n.d. | | 10.5 | |
| $R_{free}$ (%)† | 18.7 | | 19.9 | | 20.5 | |
| $R_{free}$ (%)† ($I/\sigma I > 2$) | 15.3 | | n.d. | | 16.9 | |
| *B* factors‡ | 14.01, 17.61, 17.55 | | 11.83, 13.65, 9.85 | | 14.50, 18.86, 21.51 | |
| Residues | 327 (5 to 331) | | 328 (4 to 331) | | 328 (4 to 331) | |
| Water molecules§ | 490 (30) | | 413 (86) | | 413 (50) | |
| Rounds REFMAC[15] | 12 | | 21 | | 17 | |
| Rounds SHELXL[16] | 10 | | 0 | | 9 | |
| Unit cell (Å) | $a = 46.67$, $b = 70.91$, $c = 100.73$ | | $a = 46.81$, $b = 71.66$, $c = 101.63$ | | $a = 46.78$, $b = 71.19$, $c = 101.25$ | |
| Resolution shell (Å) | 1.37–1.35 | 25.0–1.35 | 1.58–1.50 | 30.0–1.50 | 1.48–1.40 | 30.0–1.40 |
| Measurements | 9,310‖ | 404,650 | 5,146 | 267,694 | 6,601 | 344,241 |
| Average $I/\sigma I$ | 1.8 | 8.4 | 3.4 | 7.3 | 2.2 | 3.6 |
| Unique reflections | 1,595 | 69,285 | 3,572 | 46,597 | 4,482 | 55,209 |
| Completeness (%) | 43.0 | 92.2 | 57.3 | 89.7 | 50.6 | 85.3 |
| $I/\sigma I > 3$ data only (%) | 6.0 | 58.2 | 12.6 | 55.1 | 3.4 | 47.3 |
| $R_{merge}$ (%)¶ | 29.0 | 7.8 | 20.0 | 6.9 | 34.3 | 11.4 |

n.d., not determined.
*$R_{cryst} = \Sigma||F_{obs}| - |F_{calc}||/\Sigma|F| \times 100$
†$R_{free}$ = based on 5% of the total reflections.
‡Average *B* factors in order: main-chain, side-chain and substrate.
§Total number of water molecules (followed by the number of those half occupied).
‖Estimated value.
¶$R_{merge} = \Sigma_j \Sigma_h |I_{hj} - \langle I_h \rangle| / \Sigma_j \Sigma_h \langle I_h \rangle \times 100$

necessarily reduce the electron density on the β-lactam nitrogen atom, and thereby stabilize the C–S bond against fragmentation (Fig. 4). This type of fragmentation has been found in penicillins and monocyclic lactams in reactions that cause positive polarization of the sulphur atom[13,14]. On the other hand, such reduction of electron density on the nitrogen in ACV would inhibit the reaction that forms the β-lactam C–N bond. Thus the timing of these hydrogen-bonding interactions, and the positioning of these water moelcules, may well have a crucial role in the overall reaction.

The introduction of dioxygen as a high-pressure gas, coupled to the use of anaerobically grown crystals containing modified substrates, provides an approach to the structural exploration of the reaction cycles of these oxidative enzymes. This methodology allows the acquisition of a series of three-dimensional electron density 'snapshots' at selected points along the reaction pathway. In this way we have obtained structures of the enzyme–substrate complex[4], the complex of enzyme, substrate and NO as an analogue of dioxygen[4], and now the enzyme–bicyclic product complex, and—using a modified substrate—an enzyme–monocyclic product complex. □

## Methods

### Oxygenation experiments

A device suitable for exposing crystals to oxygen at pressures up to 60 bar was designed and built (N.I.B. *et al.*, manuscript in preparation). Crystals of IPNS·$Fe^{2+}$·ACV and IPNS·–$Fe^{2+}$·ACmC were grown under anaerobic conditions as reported previously[3]. Exposed crystals were prepared by rapidly transferring a single glass coverslip bearing a drop of solution containing crystals to the pressure vessel of the 'bomb'. The crystals were reacted by diffusion with 20- and 40-bar oxygen for a range of reaction times (5–640 min), then removed from the 'bomb' and rapidly frozen. Safety precautions were taken to minimize the risk of fire and explosions with high-pressure oxygen. Ultraviolet spectra of single crystals were recorded as described[15].

### Data collection

Data were collected at 100 K using synchrotron radiation and MAR Research detectors at DESY/EMBL beamline BW7B and SRS Daresbury beamline 9.6 (Table 1). Crystals were approximately 0.5 mm × 0.2 mm × 0.1 mm in size. Data were collected in dose mode, taking ~30 s per exposure.

### Structure determination

For all structures, data were processed with DENZO and SCALEPACK[16], and refined with the CCP4 suite of programs[17]. For the two exposed structures, final refinement was

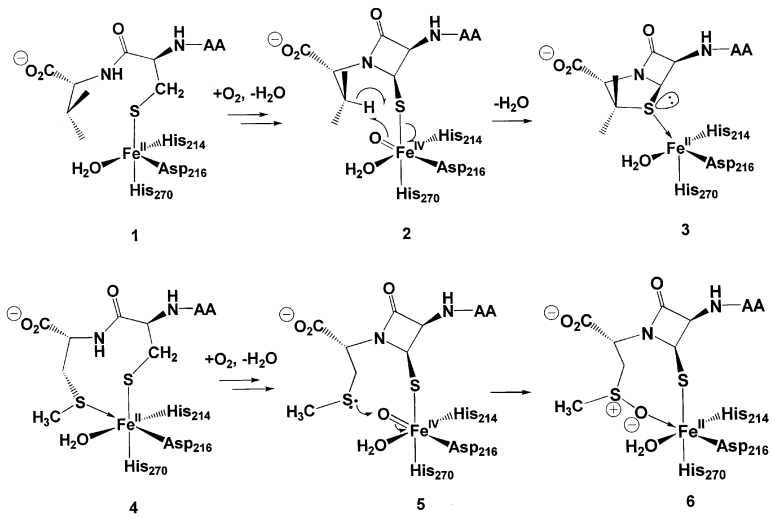


**Figure 2** Proposed mechanisms for the oxidation of ACV and ACmC to bicyclic and monocyclic products, respectively. See text for details of compounds **1**–**6**. AA, L-δ-(α-aminoadipoyl).

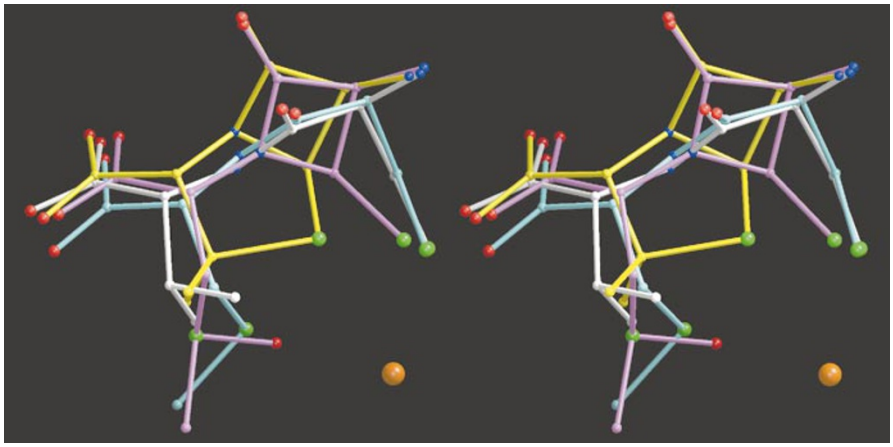

**Figure 3** Stereo views of the two substrates and two products overlaid. The key regions that participate in the reaction and the iron atom (orange) are shown; the aminoadipoyl side chain, which does not move significantly, is omitted for clarity. Shown are ACV (white), IPN (yellow), ACmC (blue) and its monocyclic sulphoxide product (pink). Figures were prepared using the programs MOLSCRIPT[20] and Raster3D (ref. 21).

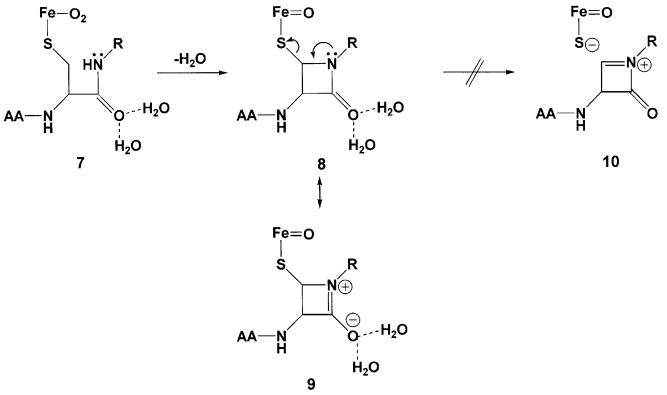


**Figure 4** The β-lactam ring is stabilized against fragmentation by hydrogen bonds from well-ordered water molecules observed in both the product structures. Such water are molecules absent from the unexposed IPNS·$Fe^{2+}$·ACV and IPNS·$Fe^{2+}$·ACmC complexes. Movement of the cysteinyl carbonyl group upon oxygen binding (**7**) and β-lactam formation enable hydrogen bonding of the carbonyl oxygen to two water molecules (**8**. This would reduce the electron density on the β-lactam nitrogen atom (**9**) and so stabilize the C–S bond against fragmentation (**10**). *R* is the remaining portion of either the D-valine or D-*S*-methylcysteine residue.

undertaken using SHELXL98 (ref. 18). Initial structures were obtained by rigid-body refinement of the IPNS·$Fe^{2+}$·ACV main-chain residues into the new unit cell. Electron-density maps were interpreted using program O (ref. 19). The iron–ligand bond lengths were unrestrained throughout refinement, and there were no Ramachandran outliers. Restraints for IPN and the monocyclic sulphoxide were calculated from models obtained from the Cambridge Structural Database. For the two exposed structures, all non-hydrogen atoms were refined anisotropically.

Water molecules, the iron atom and sulphate ions were added during the course of refinement. For each of the three structures, the IPNS·$Fe^{2+}$·ACV main-chain residues were used as the starting model for refinement. In all cases, electron density for the substrate-derived species in the active site was clearly visible throughout refinement. For the IPNS·$Fe^{2+}$·IPN structure, IPN was modelled in during the initial REFMAC[17] refinement, but for the subsequent refinements with SHELXL98 (ref. 18), a model with an IPN·ACV occupancy ratio of 70:30 was used. For the unexposed IPNS·$Fe^{2+}$·ACmC structure, the tripeptide was modelled in after the fifth cycle of refinement. For the exposed IPNS·–$Fe^{2+}$·ACmC structure, initial refinement fitting the unreacted substrate analogue to the active-site region showed that reaction had proceeded close to completion. Thus the monocyclic species was modelled in 100% occupancy after the ninth cycle of refinement.

Received 30 April; accepted 16 August 1999.


1. Baldwin, J. E. & Abraham, E. Biosynthesis of penicillins and cephalosporins. *Nat. Prod. Rep.* **5,** 129–145 (1988).
2. Baldwin, J. E., Adlington, R. M., Moroney, S. E., Field, L. D. & Ting, H. H. Stepwise ring closure in penicillin biosynthesis. Initial beta-lactam formation. *J. Chem. Soc. Chem. Commun.* 984–986 (1984).
3. Roach, P. L. *et al*. Anaerobic crystallisation of an isopenicillin N synthase. Fe(II). substrate complex demonstrated by X-ray studies. *Eur. J. Biochem.* **242,** 736–740 (1996).
4. Roach, P. L. *et al*. Structure of isopenicillin *N* synthase complexed with substrate and the mechanism of penicillin formation. *Nature* **387,** 827–830 (1997).
5. Hajdu, J. & Andersson, I. Fast crystallography and time-resolved structures. *Annu. Rev. Biophys. Biomol. Struct.* **22,** 467–498 (1993).
6. Kriauciunas, A. *et al*. The functional role of cysteines in isopenicillin N synthase. *J. Biol. Chem.* **266,** 11779–11788 (1991).
7. Berendzen, J. *et al*. Crystal structures of reaction intermediates in cytochrome P450. *Biophys. J.* **74,** A250 (1998).
8. Schlichting, I. *et al*. Crystal structures of intermediates occurring along the reaction pathway of cytochrome P450(cam). *FASEB J.* **11,** P2 (1997).
9. Lee, S.-K., Nesheim, J. C. & Lipscomb, J. D. Transient intermediates of the methane monooxygenase catalytic cycle. *J. Biol. Chem.* **268,** 21569–21577 (1993).
10. Baldwin, J. E., Adlington, R. M., Domayne-Hayman, B. P., Ting, H.-H. & Turner, N. J. Stereospecificity of carbon-sulphur bond formation in penicillin biosynthesis. *J. Chem. Soc. Chem. Commun.* 110–113 (1986).
11. Baldwin, J. E. & Bradley, M. Isopenicillin N synthase: mechanistic studies. *Chem. Rev.* **90,** 1079–1088 (1990).
12. Rigau, J. J., Bacon, C. C. & Johnson, C. R. The stereochemistry of oxidation at sulfur. Oxidation of 2-methylthiolane. *J. Org. Chem.* **35,** 3655–3657 (1970).
13. Baldwin, J. E. *et al*. Identification and characterisation of shunt metabolites from isopenicillin N synthase. *J. Chem. Soc. Chem. Commun.* 1125–1128 (1988).
14. Baldwin, J. E. *et al*. γ-Lactam formation from tripeptides with isopenicillin N synthase. *J. Chem. Soc. Chem. Commun.* 1128–1130 (1988).
15. Hadfield, A. & Hajdu, J. A fast and portable microspectrophotometer for protein crystallography. *J. Appl. Crystallogr.* **26,** 839–842 (1993).
16. Otwinowski, Z. & Minor, W. Processing of X-ray diffraction data collected in oscillation mode. *Methods Enzymol.* **276,** 307–326 (1997).
17. CCP4. The CCP4 suite: programs for protein crystallography. *Acta Crystallogr. D* **50,** 760–763 (1994).
18. Sheldrick, G. M. & Schneider, T. R. SHELXL: High-resolution refinement. *Methods Enzymol.* **277,** 319–343 (1997).
19. Jones, T. A., Zou, J. Y., Cowan, S. W. & Kjelgaard, M. Improved methods for building protein models in electron density maps and the location of errors in these models. *Acta Crystallogr. A* **47,** 110–119 (1991).
20. Kraulis, P. J. Molscript—a program to produce both detailed and schematic plots of protein structures. *J. Appl. Crystallogr.* **24,** 946–950 (1991).
21. Merritt, E. A. & Murphy, M. E. P. Raster3D Version 2.0—a program for photorealistic molecular graphics. *Acta Crystallogr. D* **50,** 869–873 (1994).


## Acknowledgements

We thank K. Harlos, C. Schofield, A. Long, J. Elkins, J. Ogle, P. Wright, R. Wilmouth, S. Lee, A. Salmeen, J. Pitt, J. Keeping and the scientists at SRS Daresbury, EMBL Hamburg and ESRF Grenoble for help and discussions. Financial support was provided by the MRC, BBSRC and ESPRC. P.L.R. thanks the Royal Society for financial support. N.I.B. was supported by a German DAAD fellowship. P.J.R. thanks the Rhodes Trust for support.

Correspondence and requests for materials should be addressed to J.E.B. (e-mail: jack.baldwin@chem.ox.ac.uk.). The crystallographic coordinates and structure factors have been deposited in the Brookhaven Protein Data Bank (accession nos 1qje and r1qjesf for IPNS·$Fe^{2+}$·IPN, 1qiq and r1qiqsf for unexposed IPNS·$Fe^{2+}$·ACmC, and 1qjf and r1qjfsf for exposed IPNS·$Fe^{2+}$·ACmC).